Veterinary Microbiology 230 (2019) 32–44

Contents lists available at ScienceDirect

Veterinary Microbiology

journal homepage: www.elsevier.com/locate/vetmic

In vivo cellular and molecular study on duck spleen infected by duck Tembusu virus

Xuejing Sun, Wenqian Li, Enxue Liu, Haixiang Huang, Taozhi Wang, Xindong Wang, Yonghong Shi, Ping Yang, Qiusheng Chen*

Ministry of Education Joint International Research Laboratory of Animal Health and Food Safety, College of Veterinary Medicine, Nanjing Agricultural University, Nanjing, Jiangsu Province, PR China

ARTICLE INFO

Keywords:
Duck Tembusu virus
Spleen
Pathogenicity
RNA-seq
Lymphocyte homing

ABSTRACT

Duck Tembusu virus (DTMUV) is a novel member of flavivirus with the highest viral loads in the spleen. Six-month egg-laying shelducks were intramuscularly injected with DTMUV strain XZ-2012. Morphological analysis revealed the presence of vacuolar degeneration in the periellipsoidal lymphatic sheaths (PELS) of spleen white pulp following infection, especially from 12 hpi to 3 dpi. Ultrastructural images showed an obvious swelling of cells and their mitochondria and endoplasmic reticulum. Using RNA-seq analysis, the expression levels of RIG-I like receptors (RLRs), downstream IRF7 and proinflammatory cytokines IL-6 from RIG-I signaling pathway were non-apparently upregulated at 2 hpi and apparently at 3 dpi, while MHC-II expression was obviously down-regulated at 2 hpi. The expression levels of downstream antiviral cytokines type-I IFNs, anti-inflammatory cytokines IL-10, cell adhesion molecules (CAMs), chemokines and their receptors associated with lymphocyte homing were significantly upregulated at 3 dpi. The population of lymphocyte was increased at 6 dpi. The immune function of spleen was recovered starting from 9 dpi. These findings of this study suggest that DTMUV invaded into the spleen via RIG-I signaling pathway and enhanced immune evasion by inhibiting MHC-II expression during the early stage of infection. Additionally, DTMUV induced PELS lesions through activating IL-6 expression. Furthermore, DTMUV increased the expression levels of RLRs, antiviral type-I IFNs, lymphocyte homing-related genes and proteins as well as the number of lymphocytes in the infected duck spleen. Taken altogether, this study provides new insights into the cellular and molecular mechanisms of DTMUV infection in duck spleen.

1. Introduction

Duck Tembusu virus (DTMUV), a pathogenic member of flavivirus family, was first discovered in the coastal provinces of South-Eastern China in 2010 (Teng et al., 2010). DTMUV can be harmful to most egg-laying ducks, meat ducks, chickens and geese (Chen et al., 2011; Huang et al., 2013; Ti et al., 2015; Wan et al., 2012; Yun et al., 2012a, b; Zhang et al., 2015), which results in high mortality, retarded growth and reduced egg production (Cao et al., 2011).

DTMUV is a positive-sense single-stranded RNA virus and shares a similar pathogenicity with other flaviviruses (Su et al., 2011; Wan et al., 2010; Yan et al., 2011). After infecting animals, the virus spreads through bloodstream and induces viremia. Subsequently, the virus can be transmitted into the spleen and replicates in large quantities. Eventually, the virus becomes active and invades other organs and tissues, even the blood-brain barrier (Samuel and Diamond, 2006; Sejvar et al., 2003). The lesions of DTMUV infection are often characterized by swelling, internal bleeding and follicular hyperemia, atrophy, and egg yolk peritonitis. The long-term infection may cause nervous system disease and even death.

As the largest secondary lymphoid organ, the spleen plays a pivotal role in filtering and destroying specific pathogens. Of note, the spleen accumulates a high viral load of flaviviruses, including DTMUV (Carson et al., 2006; Garcia et al., 2011; Jiang et al., 2012; Kato et al., 2014; Wu et al., 2014).

The majority of DTMUV studies have focused on its isolation, genome detection and diagnostic techniques. However, the cellular and molecular mechanisms underlying DTMUV infection in duck spleen remain largely unknown. Given the sequencing throughput, RNA sequencing (RNA-seq) can generate a large quantity of transcriptomic data within biological samples. RNA-Seq has been used to analyze the changes in gene expression over time and compare the differences in

* Corresponding author at: College of Veterinary Medicine, Nanjing Agricultural University, Nanjing, Jiangsu Province, 210095, PR China.
E-mail address: chenqsh305@njau.edu.cn (Q. Chen).

https://doi.org/10.1016/j.vetmic.2018.12.003
Received 22 September 2018; Received in revised form 4 December 2018; Accepted 4 December 2018
0378-1135/

gene expression between two groups (e.g. treatment and control) (Chu and Corey, 2012; Maher et al., 2009; Wang et al., 2009). Therefore, this study aimed to investigate the morphological and transcriptional changes in duck spleen following DTMUV infection. In addition, we attempt to identify the genes and pathways associated with DTMUV infection. Undoubtedly, this study could provide a novel theoretical foundation for the invasion process of DTMUV in duck spleen.

2. Materials and methods

2.1. Preparation of virus samples

Duck Tembusu virus (DTMUV) XZ-2012 strain was isolated and cultured in BHK-21 cells (Wang et al., 2015). After freeze thawing for three times, the virus (200 μL) was injected into the allantoic cavity of 10-day-old SPF duck embryos. Allantoic fluid was collected after 3–4 days of incubation, followed by RT-PCR assay. $TCID_{50}$ values of positive samples were calculated using Reed-Muench method (Reed and Muench, 1938) and then stored in −80℃ until further analysis.

2.2. Infection of experimental animals

A total of 190 healthy egg-laying shelducks (Nanjing, China) at 6 months old, negative of any DTMUV and their antibody in vivo using RT-PCR and ELISA (Jiangsu Meimian industrial Co., Ltd., China) were divided into treatment groups and control groups. All ducks in the treatment groups (n = 15 in each group) were intramuscularly injected virus at dose of 10^4 $TCID_{50}$ ($TCID_{50}$ in this study was $10^{-5.7}$/100 μL). Following infection, the ducks were euthanized at 2 and 12 h, post-infection (hpi) as well as 1, 3, 6, 9 and 18 days post-infection (dpi). Meanwhile, the ducks in control group were euthanized after injected with the same volume of 0.9% NaCl at 0 h (n = 15 in each group) and the same 7 time points (n = 10 in each group).

2.3. Haematoxylin and eosin (H&E) staining

Spleen samples were obtained and sectioned immediately following a post-mortem. Subsequently, the samples were fixed in 4% buffered paraformaldehyde for 24–48 h, embedded in paraffin, and sectioned at 5 μm thickness using a Leica microtome (Germany). These sections were then stained with H&E.

2.4. Transmission electron microscopy (TEM)

The spleens were cut into 1 mm^3 blocks, and then fixed by immersion in 2.5% glutaraldehyde diluted with 0.01 M phosphate-buffered saline (PBS, pH 7.4) at 4 ℃ overnight. After incubation, the samples were post-fixed in 1% osmium tetroxide in the same buffer for 60 min. Next, the samples were dehydrated in ascending concentrations of ethyl alcohol, infiltrated with propylene oxide-Araldite mixture, and embedded in Araldite. Finally, the ultrathin sections (50 nm) were stained with uranyl acetate and lead citrate for 20 min each.

2.5. Immunofluorescence

The spleen samples, fixed in 4% paraformaldehyde for 24–48 h, were embedded in paraffin, and sectioned to a 3 μm thickness using a Leica microtome (Germany). Briefly, after deparaffinization and washing with PBS, the antigen sections were exposed to citric acid buffer at 121℃ for 10–15 min. Then, they were inactivated with endogenous peroxidase by covering them with 3% hydrogen peroxide for 10 min. After being washed with PBS, the sections were blocked with 5% BSA for 1 h at 37℃ and incubated with the rabbit anti-DTMUV XZ-2012 E protein polyclonal antibody (Homemade polyclonal antibody) for 16 h at 4℃. After washing with PBS, the sections were incubated for 1 h with Alexa Fluor 488 affinipure goat anti-rabbit IgG (H + L) (Fcmacs Biotech, China). After washing, the sections were stained with DAPI (4′, 6-diamidino-2-phenylindole) (Boster Biotech, China) for 5 min in the dark. Then the samples were covered and observed with a fluorescence microscope (Olympus DP73, Japan).

Well-stained sections were observed under a light microscopy, and photographed using an Olympus DP73 microscopy equipped with digital camera. For TEM examination, the stained sections were observed and digitally photographed with a Hitachi H-7650 transmission electron microscope (Hitachi, Japan).

2.6. RNA extracting, cDNA library construction and sequencing

RNA was extracted from the duck spleens using Trizol method (TransGen Biotech, China). The quality of RNA was measured using ND-1000 spectrophotometer (Thermo, USA) and Agilent2100 bioanalyzer in order to meet the requirement of library construction. mRNA was enriched by magnetic beads using oligo (dT) and fragmented with fragmentation buffer. cDNA was then synthesized using the fragmented mRNA as template, followed by purification with QiaQuick PCR kit. Through terminal repair, plusing poly(A) and sequencing joints, the construction of eight cDNA libraries was completed after PCR amplification and gel extraction. The constructed cDNA libraries were then sequenced by Illumina HiSeqTM 2500. The samples of control, 2hpi, 12hpi, 1dpi, 3dpi, 6dpi, 9dpi and 18dpi were named as C, D1, D2, D3, D4, D5, D6 and D7, respectively. The construction of cDNA library and sequencing were performed by Genedenovo Biotechnology Co. Ltd, Guangzhou, China. All data would be submitted into NCBI Sequence Read Archive (SRA, http://www.ncbi.nlm.nih.gov/Traces/sra/) (SRA accession: PRJNA509092).

2.7. Data analysis and differentially expressed genes (DEGs)

Raw reads were pre-processed into clean reads by removing the reads containing adapter, ploy-N and rRNA and low-quality reads ($Q \leq 20$). High-quality clean reads were then mapped respectively to mallard (*Anas platyrhynchos*) genome sequence (GCF_000355885.1) by using TopHat2 software (Kim et al., 2013). After that, the transcripts were assembled with cufflinks (Trapnell et al., 2010). The principal component analysis (PCA) and Pierce correlation coefficient between two samples were carried out by R language (http://www.r-project.org/). Gene expression levels were normalized according to the fragments per kilobase of transcript per million mapped reads (FPKM) method. DEGs statistics were analyzed by edgeR software package based on R language (http://www.bioconductor.org/packages/release/bioc/html/edgeR.html), in order to compare the statistical difference between two groups. FDR corrected P value < 0.05 and $|\log_2$ Fold Change$| > 1$ were used to determine the significant levels of DEGs.

2.8. Annotation and function prediction of DEGs

All DEGs were subjected to Gene Ontology (GO) and Kyoto Encyclopedia of Genes and Genomes (KEGG) annotations. GO terms with $P < 0.05$ were considered significantly enriched among the DEGs. The main biological functions of DEGs were determined according to GO function enrichment analysis.

KEGG is a database of biological systems that links genomes to life through the process of Pathway mapping. After multiple inspection and correction, pathways with $P < 0.05$ in KEGG (http://www.genome.jp/kegg/) were defined as significantly enriched pathways for the DEGs. In addition, pathway significance enrichment analysis was used to identify the significant metabolic pathways or signal transduction pathways regulated by DEGs.

2.9. Weight gene co-expression network analysis (WGCNA)

WGCNA is a systems biology approach for exploring gene networks

Table 1
Primers used in the RT-qPCR.

Target genes	Primer sequences (5'-3')	Amplicon length (bp)
MHC-2	F: GGACCCGTGGATTTGTGTG R: ACACTCCCCTGGGAATCCT	131
DDX58/RIG-1	F: ACCCTTACCTCGCTCTCCAT R: TTACCAACTCCAACAGAAGC	170
IFIH1/MDA5	F: TTGGTGCTGGACACAACAGT R: GTGACAAGGCCATAGCGAAT	169
DHX58/LGP2	F: AGCTGGCAAGTGAAAGAAGC R: CCTGAAATTGGGGTTGATGT	162
MB21D1/cGAS	F: CTTGGCTTTGGAAGTTCAGC R: AGAAAGAGATTCGCCAGGTG	176
TMEM173/STING	F: TATGCCATGTCTCAGGACGA R: TCGGCTTCTATCAGCTCCTC	158
IRF7	F: CAACATAATGGGGCGAGAAG R: CAGGGACTGGTAGGTCAGCA	162
IL-6	F: CAACGACGATAAGGCAGATG R: CCCTCACGGTTTTCTCCATA	171
STAT1	F: GCAGCTGAGAACATTCCTGA R: GGGGTGGACTTCAGAAACAG	180
IL-10	F: CTGACCTCCTACCAGCGAAG R: CTCCATGTAGAACCGCATCA	179
IFNA	F: TCCGCATCGTTGTCTAAGAG R: TGTTCTAGAGCTGCCCCATC	171
VCAM1	F: GCTAACATGGACTTTGAGCCC R: GAGGGTTGCCTTCCACTGTA	121
ITGB2	F: GAAGAGCAGCCTGACCAAAC R: TGCCGTAGATCTGCTTGTTG	244
CCL21	F: GCGAGAGGACCAGTTTAGAG R: GCTGGTGAGAGAGGAGCAGA	140
DTMUV	5'-AAGCGAGCACCTACCACA-3' 5'-TGCCCCATATCAACTCCAGA-3'	157
β-actin	F: GATCTGGCACCACACCTTCT R: GCTACATACATGGCTGGGGT	153

instead of individual genes (Hollender et al., 2014). R language package was used to perform WGCNA (Langfelder and Horvath, 2008). After filtering the low quality and unstable genes (FPKM of each samples < 1), DEGs with similar expression patterns were clustered into a module. These modules were defined as clusters of highly interconnected genes, in which the genes within the same cluster have high correlation coefficients among each other. Additionally, the correlation between modules and the connectivity between genes within each module were analyzed. The related genes from appropriate modules were selected for further analysis.

2.10. RT-qPCR validation

DEGs related to virus invasion and immune response and DTMUV E gene (Accession No.: KM188953.1) were selected for RT-qPCR validation. Primers sequences were designed using Primer 3.0 software (Table 1). The β-actin gene of duck was used as internal reference. RNA was extracted from eight duck spleen samples and reverse transcribed into cDNA. RT-qPCR was performed on Applied Biosystems 7500 Real-Time PCR Systems (ABI, US) using SYBR Green MasterMix-Low ROX Kit (abm, China). All samples were measured in triplicate. The relative quantification of target gene expression was calculated by $2^{-\Delta\Delta Ct}$ method. Heatmap was drawn using an online tool (http://www.omicshare.com/).

2.11. Western blotting

The mAbs of MHC-2, RIG-1, MDA5, LGP2, cGAS, STING, IRF7, IL-6, IL-10, STAT1, IFNA, VCAM-1, CCL21, Integrin β2 and β-actin (ABclonal Technology, China) were used as primary antibodies for Western blot analysis. Total proteins were extracted from duck spleen with cold lysis buffer (50 mM Tris – HCl (pH 7.6), 150 mM NaCl, 1% Nonidet-P40, 1% sodium deoxycholate, 0.1% SDS and 0.05 mM PMSF) and allowed to incubate for 30 min. Total protein concentrations were determined using BCA Protein Assay kit (Thermo Fisher Scientific, USA). The protein samples (20 μg per lane) were detected with 10% SDS-PAGE, and the separated proteins were transferred onto polyvinylidene difluoride (PVDF) membrane (Transgen Biotech, China). Subsequently, the membrane was blocked with 5% skimmed milk powder for 2 h, followed by overnight incubation with primary antibody (1:100) at 4 °C. After washing in TBST buffer, the membranes were incubated with horse radish peroxidase (HRP) conjugated secondary goat anti-rabbit IgG (H + L) (1:5000, Transgen Biotech, China) for 1 h. After washing in TBST buffer, HRP signals were detected by an enhanced luminol-based chemiluminescent substrate (Tanon Science & Technology, China). The expression levels of target proteins were quantified in ImageJ software calculating the grayscale value.

2.12. Data analysis

All data were expressed as mean ± standard error of the mean (SEM). The data analysis was performed using GraphPad Prism software version 5.0 with a one-way analysis of variance (ANOVA).

3. Results

3.1. The morphological and cellular lesions of the infected duck spleens

After infection, ducks showed depression at 1dpi and 3dpi, without other obvious clinical symptoms. After necropsy, the healthy duck spleen was revealed as a red-purple, triangle-shaped, substantial organ. Different degrees of obvious swelling, hyperemia and status marmoratus were observed among the infected duck spleens from 12hpi to 3dpi. Moreover, the texture of the spleens was soft and brittle (Fig. 1).

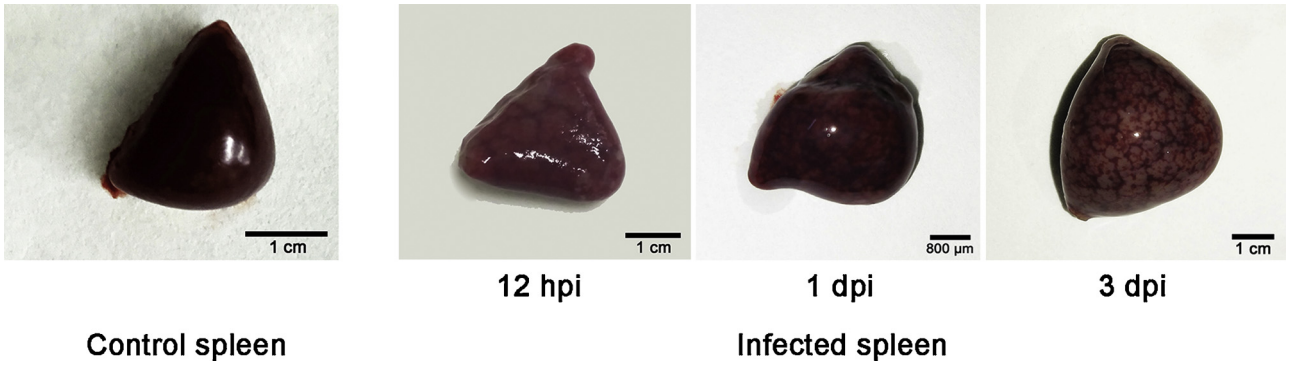

Fig. 1. Morphological characteristics in the healthy and infected duck spleens. The control duck spleen is red-purple and triangle-shaped. The infected duck spleens are swelling, hyperemia and status marmoratus. Bar = 1 cm, 1 cm, 800 μm, 1 cm. (For interpretation of the references to colour in this figure legend, the reader is referred to the web version of this article).

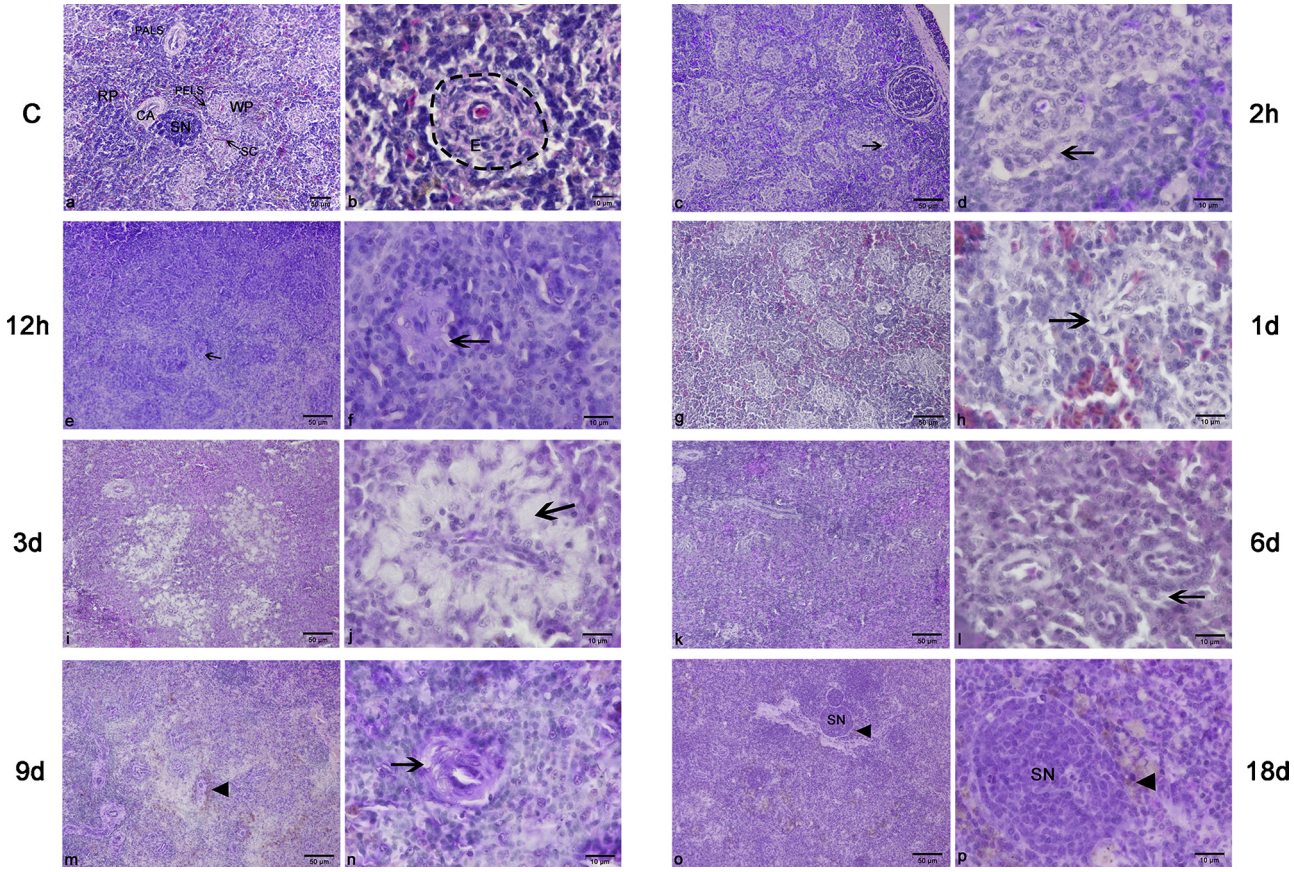

Fig. 2. Histopathologic characteristics of the duck spleens (HE staining). (a–b) The histological characteristics in normal duck spleen. (c–j) The vacuolar degeneration (→) is mainly seen in central artery and the border between ellipsoid and PELS from 2hpi to 1dpi. and the inflammatory area in PELS (→) is gradually enlarged on 3 dpi. (k–l) On 6dpi, the inflammatory area (→) is recovered. The number of lymphocytes was increased. (m–p) A large amount of hemosiderin (▲) is distributed around ellipsoid on 9dpi, then is migrated into the red pulp and around splenic nodules on 18dpi. Bar = 50 μm, 10 μm. WP: white pulp; RP: red pulp; CA: central artery; SN: splenic nodule; SC: sheathed capillary; PELS: periellipsoidal lymphatic sheaths; PALS: periarterial lymphatic sheaths; E: ellipsoid (black dotted line). (For interpretation of the references to colour in this figure legend, the reader is referred to the web version of this article).

Histologically, the healthy control spleen exhibited normal structures of red pulp and white pulp. Notably, white pulp is composed of ellipsoids, periellipsoidal lymphatic sheaths (PELS), periarterial lymphatic sheaths (PALS) and splenic nodules. The endothelial cells of the sheathed capillaries surrounded by ellipsoid were cuboidal-shaped, named high endothelial venules (HEVs) (Fig. 2a and b). Compared to the control spleen, the vacuolar degeneration was observed in the central artery and the border between ellipsoid and PELS at 2 hpi and 12 hpi (Fig. 2c–f). At 1dpi, the number of erythrocytes was increased and hyperemia was induced in splenic sinus, while the vacuolar degeneration between ellipsoid and PELS was aggravated (Fig. 2g and h). At 3 dpi, the inflamed region in PELS was enlarged, and the spleen tissues surrounding ellipsoid were severely damaged and displayed light staining. At 6 dpi, the population of lymphocytes was increased, and PELS was recovered compared to the conditions observed at 3 dpi. The population of lymphocytes was increased (Fig. 2k and l). At 9dpi, a large amount of hemosiderin was found to be accumulated around the ellipsoid, and subsequently assembled in the red pulp and near the splenic nodules at 18dpi (Fig. 2m–p).

The ultrastructure of normal duck spleen appeared to have a complete cell morphology (Fig. 3a and b). At 2 and 12 hpi, the endosomes were found in the cuboidal-shaped endothelial cells of sheathed capillaries and lymphocytes. Besides, an obvious swelling of endoplasmic reticulum and vacuolated cytoplasm were observed in the endothelial cells, macrophages and lymphocytes (Fig. 3c–f). At 1 dpi, an abundant swollen endoplasmic reticulum and mitochondria, fractured mitochondrial cristae and cytoplasm vacuolation were presented in a large number of lymphocytes and macrophages (Fig. 3g and h). At 3 dpi, the cytoplasm of most cells around the sheathed capillaries exhibited vacuolation, swelling and plasmarrhexis, while the mitochondrial cristae faded out (Fig. 3i and j). At 6 dpi, the number of eosinophilic granulocytes was increased, and the number of cells that had swallowed endoplasmic reticulum was decreased, as compared to those at 3 dpi (Fig. 3k and l). From 9 dpi to 18 dpi, a proportion of erythrocytes was wrapped in the macrophages, and the basement membrane of the sheathed capillaries was thickened. Eventually, the morphology of spleen cells was completely restored (Fig. 3m–p).

3.2. DTMUV location in the spleen by immunofluorescence

The immunofluorescent results revealed the location of DTMUV in spleen at different times. It was observed that the positive reactions of the virus were present in spleen showed as dot-like particles. The positive reactions were mostly distributed in the PELS of white pulp from 2 hpi to 6 dpi. From 9 dpi to 18 dpi, the positive reactions were mostly distributed in PALS around the central artery (Fig. 4). The number of positive particles was increased first and then decreased after infection, reaching to the peak on 3dpi.

3.3. RNA-seq data analysis and DEGs identification

3.3.1. Transcriptome assembly and annotation

Eight cDNA libraries were constructed spleen samples of control (C), 2 hpi (D1), 12 hpi (D2), 1 dpi (D3), 3 dpi (D4), 6 dpi (D5), 9 dpi (D6)

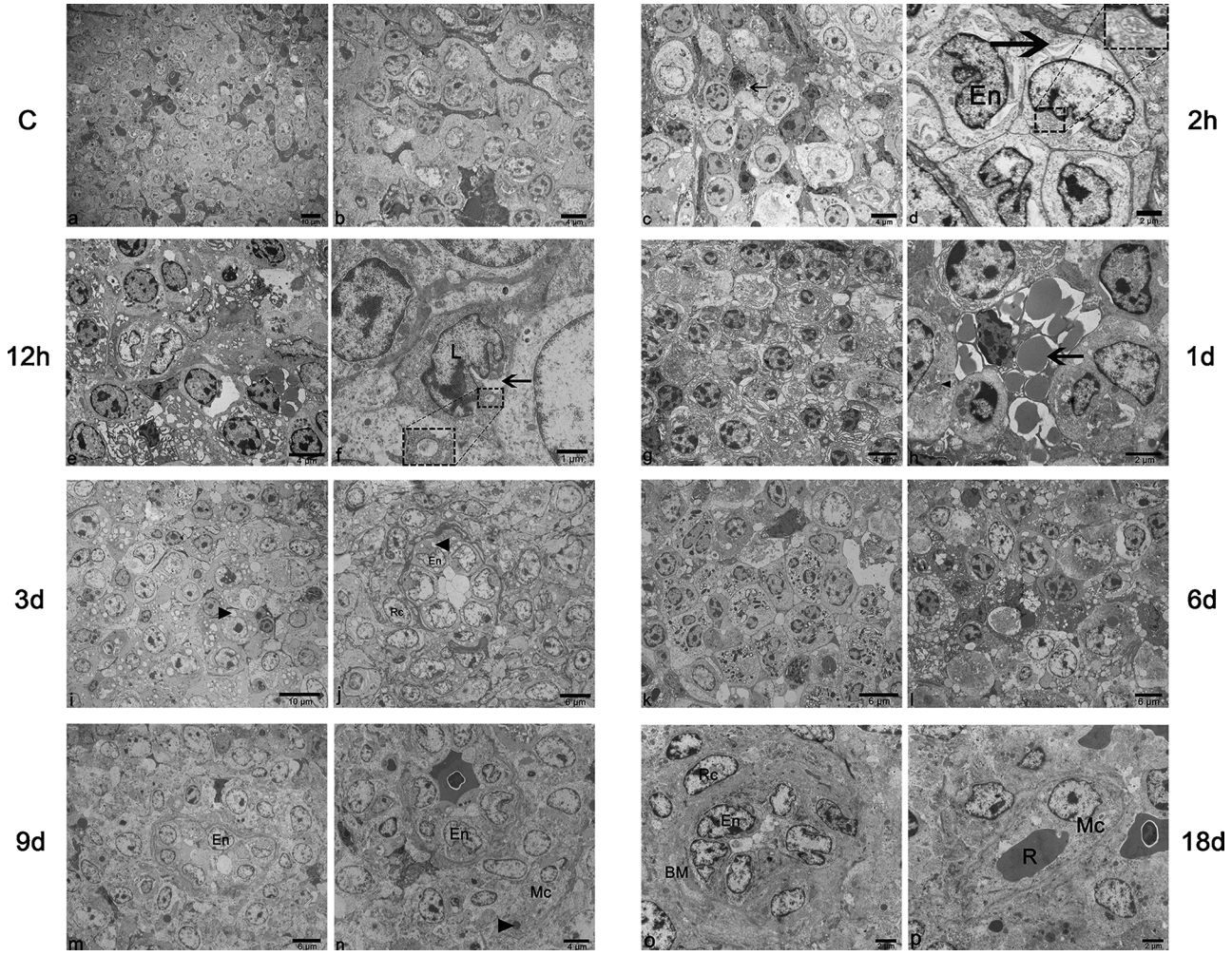

Fig. 3. Ultrastructure characteristics of the infected duck spleens (TEM). (a–b) The ultrastructure of the normal duck spleen. Bar = 10 μm, 4 μm. (c–d) At 2 hpi, the endosomes (black dotted line) in the high endothelial cells of cytoplasmic vacuolation (→). Bar = 4 μm, 2 μm. (e–f) At 12 hpi, the swelling of endoplasmic reticulum and cytoplasm vacuolization (→) in macrophages and lymphocytes. The endosomes (black dotted line) in lymphocytes. Bar = 4 μm, 1 μm. (g–h) On 1 dpi, the swollen endoplasmic reticulum and mitochondria, fractured mitochondrial cristae and cytoplasm vacuolization in lymphocytes and macrophages. Bar = 4 μm, 2 μm. (i–j) On 3 dpi, the cytoplasm vacuolation, swelling and plasmarrhexis of most cells in white pulp, The mitochondrial cristae (▲) of cells is faded away. Bar = 10 μm, 6 μm. (k–l) On 6 dpi, the number of eosinophilic granulocytes is increased, and the number of swollen cells is decreased. Bar = 6 μm, 6 μm. (m–p) From 9 dpi to 18 dpi, some of erythrocytes are wrapped in macrophages (▲). Bar = 6 μm, 4 μm, 2 μm, 2 μm. En: endothelial cell; L: lymphocyte; Rc: reticular cell; BM: basement membrane; R: red blood cell; Mc: macrophage. (For interpretation of the references to colour in this figure legend, the reader is referred to the web version of this article).

and 18 dpi (D7) after performing RNA-seq with Illumina HiSeq 2500 platform. The results of sequencing quality assessment were found to be highly reliable. The clean reads were obtained from these eight libraries, with 67.47, 64.29, 64.54, 63.81, 65.39, 54.39, 62.50 and 66.78% of the total reads were mapped to the mallard (*Anas platyrhynchos*) reference genome, respectively (Supplement Table 1). There was a total of 10572 genes in the known reference genome. The statistical results of genes in all samples showed that 14165 known genes were tested with 93.98% were mapped to the reference genes, whereas 1962 new genes were tested. Finally, a total of 16127 genes were successfully retrieved.

3.3.2. Differential gene expression

To examine the expression of each gene, their read counts were analyzed using FPKM method based on FDR < 0.05 and $|\log2FC| > 1$. In overall, 821, 694, 886, 3307, 1365, 1131 and 1166 DEGs were identified by comparing D1-D7 vs. C, respectively (Supplement Table 2 and Fig. 5). Notably, the majority of DEGs were found in D4 as compared to C.

3.3.3. Functional annotation and pathway enrichment analysis

The functional annotation of DEGs was performed by assigning them with GO terms. The results of GO analysis were divided into three main categories: cellular component (C), molecular function (F) and biological process (P). By FDR ≤ 0.05 as the threshold value, a total of 43 (4 in C, one in F and 38 in. P), 20 (5 in C, 8 in. F and 7 in. P), 42(20 in C, 6 in. F and 16 in. P), 221 (23 in C, 18 in. F and 180 in. P), 12 (8 in C, 2 in. F and 2 in. P), 107 (10 in C, 16 in. F and 81 in. P) and 23 (5 in C, 5 in. F and 13 in. P) GO terms were significantly enriched between D1-D7 vs. C, respectively. In particular, several GO terms related to immune response were enriched, such as cytokine activity (GO: 0005125), antigen binding (GO: 0003823) etc. in molecular function; response to external biotic stimulus (GO: 0043207) etc. at earlier infected time and cell adhesion (GO: 0007155), lymphocyte migration (GO: 0072676), T cell activation (GO: 0042110) etc. at later infected time in biological process.

Pathway enrichment analysis was performed for annotating the DEGs with KEGG pathways by using FDR ≤ 0.05 as a threshold value. The results demonstrated that a total of 5, 3, 3, 11, 5, 5 and 2 significantly enriched pathways were identified in D1-D7 compared to C,

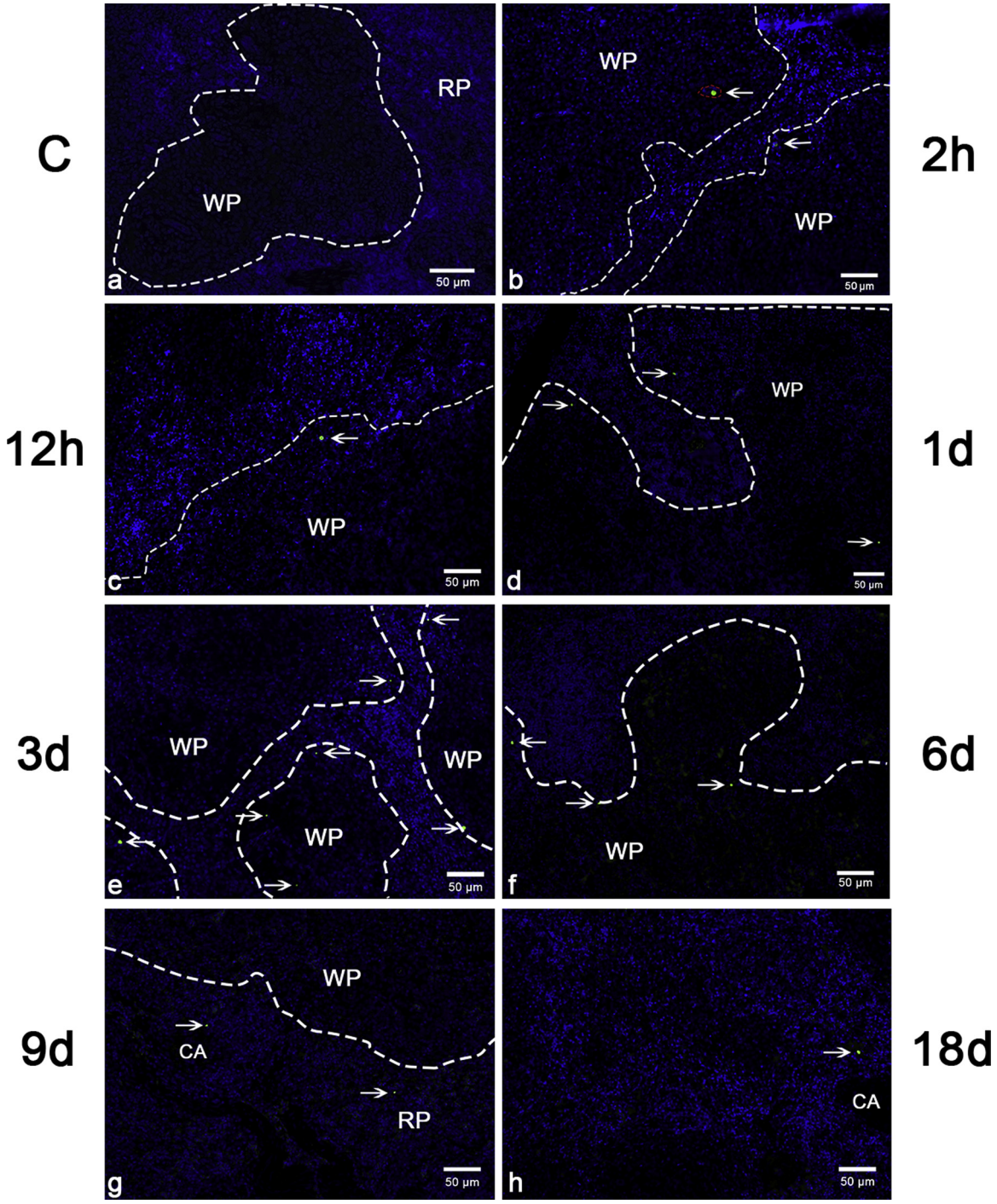

Fig. 4. Immunofluorescence results of virus in duck spleens. The positive reactions of virus are detected and dispersedly distributed as dot-like particles (→) in spleen. At 2pi, the positive reactions are found in the sheathed capillary (red dotted borders) and the periphery of white pulp (white dotted borders). Between 6hpi to 6dpi, the positive reactions are mostly distributed in the periphery of white pulp (white dotted borders). Between 9dpi to 18dpi, the positive reactions are mainly observed around the central artery. Bar = 50 μm. RP: red pulp, WP: white pulp, CA: central artery. (For interpretation of the references to colour in this figure legend, the reader is referred to the web version of this article).

respectively (Supplement Table 3). The "cytokine-cytokine receptor interaction" (ko04060) was significantly enriched in all D1-D7 groups vs. C group. "Cytosolic DNA-sensing pathway" (ko04623) and "phagosome" (ko04145) etc. that related to viral invasion were significantly enriched in D1-vs-C and D4-vs-C. "Cell adhesion molecules (CAMs)" (ko04514) and "ECM-receptor interaction" (ko04512) etc. that related to lymphocytes migration were significantly enriched as compared with the later stage of infection. The "protein processing in endoplasmic reticulum" (ko04141) and "protein export" (ko03060) were significantly enriched in D5 vs. C. Furthermore, "neuroactive ligand-receptor interaction" (ko04080) was significantly enriched after 3dpi (Fig. 6).

3.3.4. WGCNA of DEGs

Before conducting WGCNA, low-quality noisy data of 4684 genes (FPKM value of each sample ≤ 1) were filtered out, remaining 12,350 valid genes. All the genes were clustered into different modules according to their gene expression patterns. As a result, a total of 15

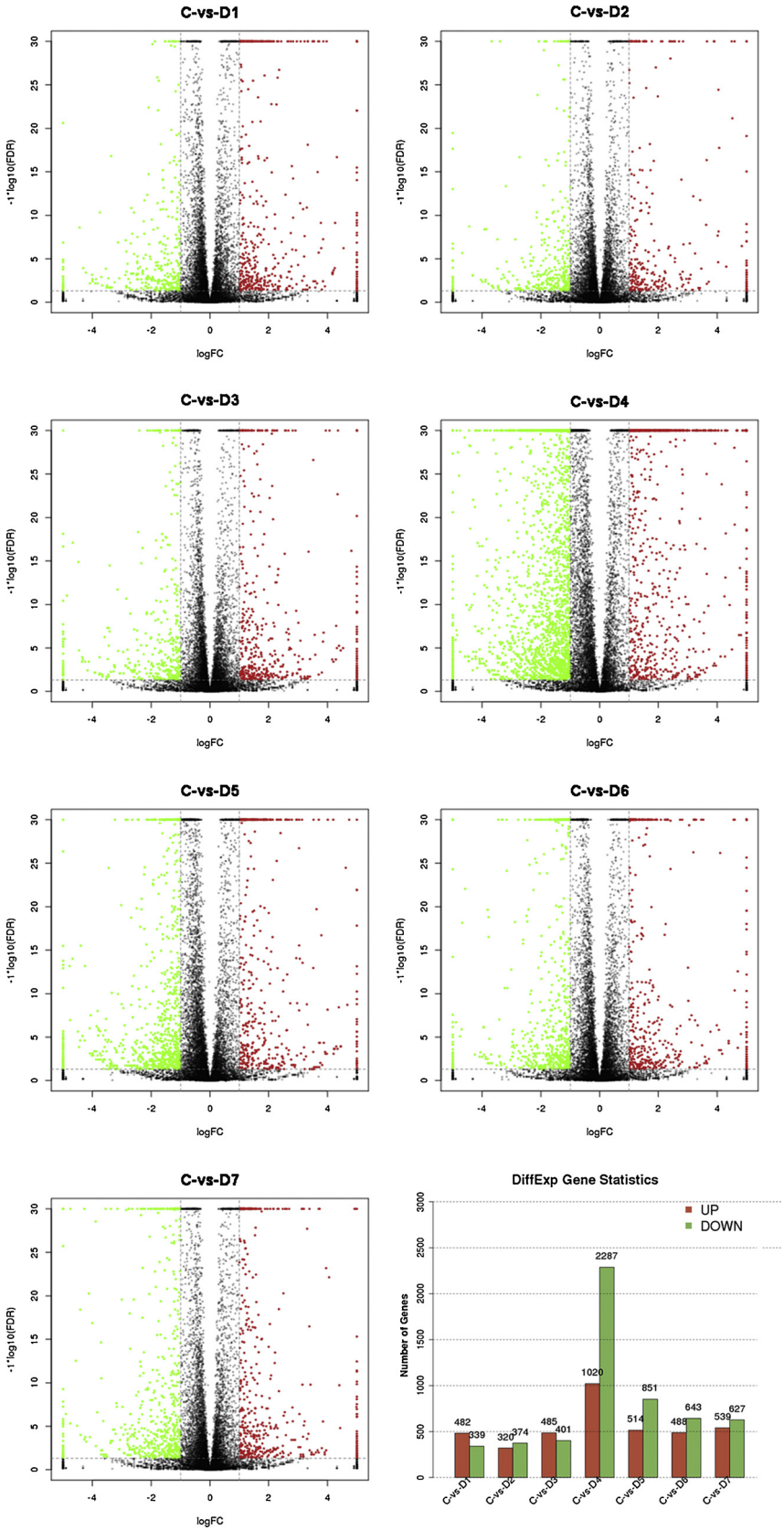

Fig. 5. Volcano plot and histogram of number of DEGs. Red is up-regulated genes, green is down-regulated genes. The majority of DEGs are assigned to the pairs of C-vs-D4. (For interpretation of the references to colour in this figure legend, the reader is referred to the web version of this article).

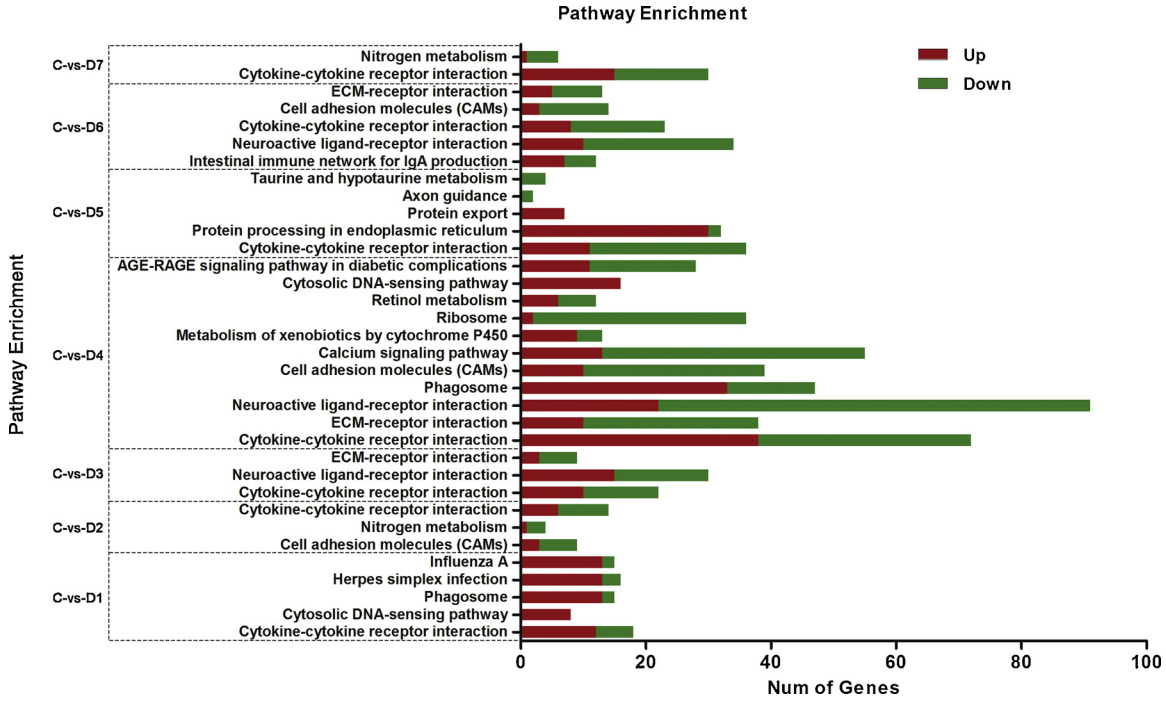

Fig. 6. Significantly enriched pathways (P ≤ 0.05) of DEGs between samples. The more pathways are assigned to the pairs of C-vs-D4.

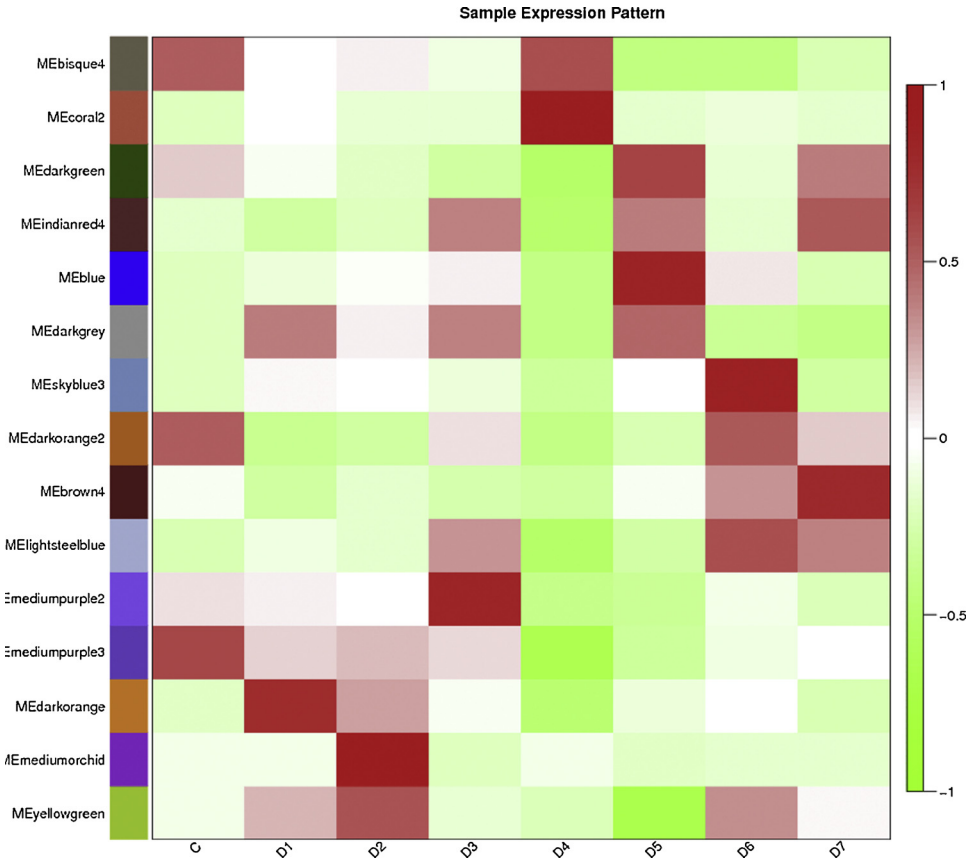

Fig. 7. Sample expression pattern. The x-coordinate represents the eight samples, the y-coordinate represents the fifteen modules. The red color represents high expression, the green color represents low expression. (For interpretation of the references to colour in this figure legend, the reader is referred to the web version of this article).

distinct modules were obtained from WGCNA (labeled by different colors) (Supplement Table 4 and Fig. 7). The correlation between modules and the connectivity between genes within each module were analyzed and visualized as heat map (As shown in Fig. 8a and b), each tree branch constituted a module, and each leaf in the branch represented one gene. The connectivity of a gene is defined as the sum of correlation coefficients with all other genes in the network. P-value of the correlation test between two modules was calculated by Student's *t*-test The smaller the p-value, the higher the similarity between two modules. The genes with higher connectivity may demonstrate greater and biological significance than others. In this study, two largest modules (i.e. mediumpurple3 and coral2) exhibited the highest

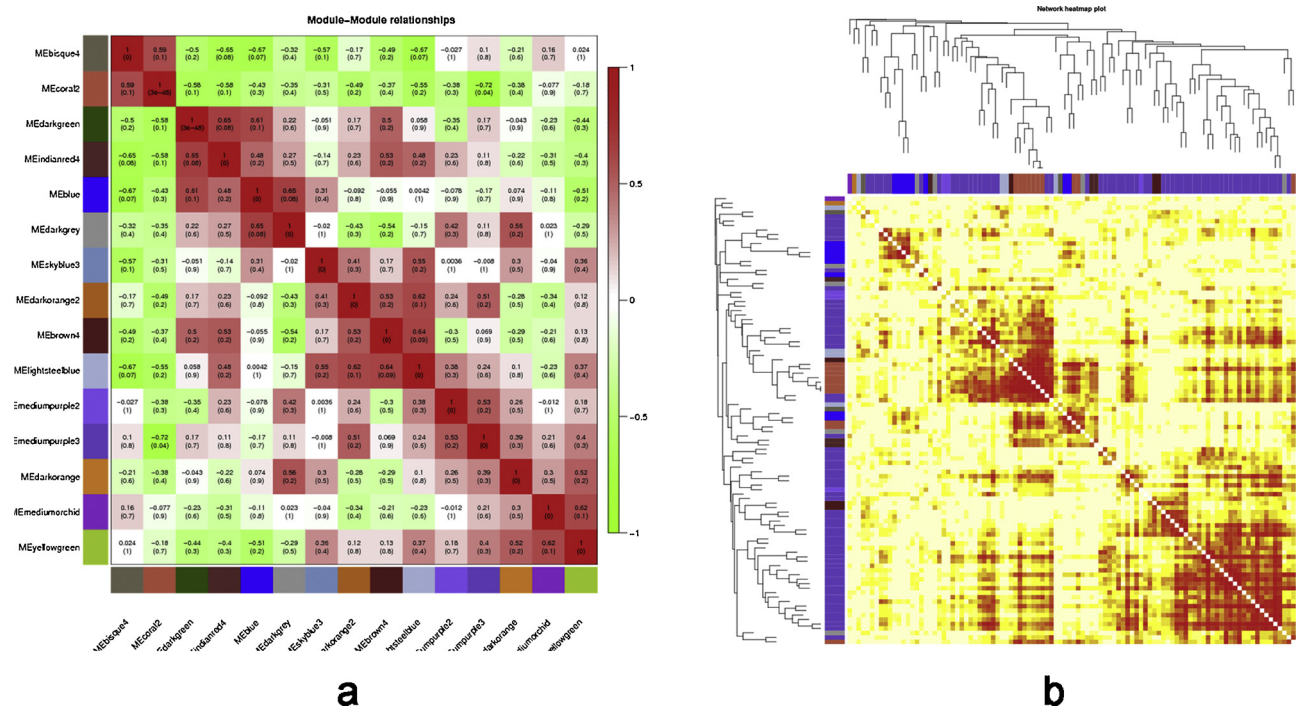

Fig. 8. The heat map of correlation between modules (a) and genes (b). (a) Each row or column represents a module. The number in the square is the correlation coefficient between the two module eigenvalues. The number in brackets is P value. The darker the square color (more red or green), the stronger the correlation. The lighter the square color, the weaker the correlation. The smaller P value, the higher the similarity between the two modules. It is found that the P value (0.04) of the correlation between mediumpurple3 and coral2 was the least, the correlation is the strongest. (b) Each row or column represents a gene. The darker the color of each point, the greater the connectivity between the two genes of corresponding row and column. It is found that the connectivity of genes of mediumpurple3 and coral2 is highest. (For interpretation of the references to colour in this figure legend, the reader is referred to the web version of this article).

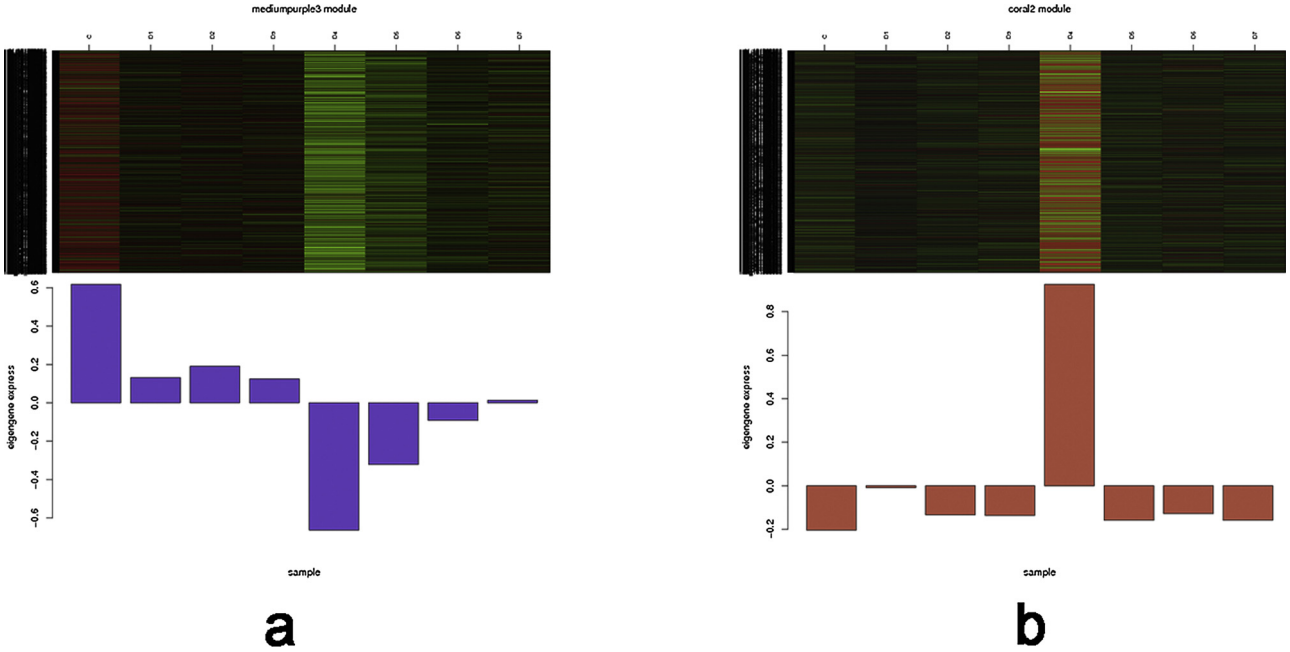

Fig. 9. mediumpurple3 (a) and coral2 (b) modules genes expression pattern. The above heat map is the expression of genes in different samples. Red is up-regulated, green is down-regulated. The below figure is the expression patterns in different samples. (For interpretation of the references to colour in this figure legend, the reader is referred to the web version of this article).

correlation and genetic connectivity, with the lowest p-values (Fig. 9).

3.3.5. Identification of DEGs and pathways that related to antiviral innate immune response and lymphocyte homing

A total of 23 significant DEGs ($|\log_2 FC| > 1$ and FDR < 0.05) were identified from mediumpurple3 or coral2 modules as well as the significantly enriched pathways associated with antiviral innate immune response and lymphocyte homing (Table 2). Seven identified DEGs of cytosolic DNA-sensing pathway (i.e. RIG-1, MDA5, cGAS, STING, downstream signal molecules LGP2 and IRF7) were associated with

Table 2
The pathways and DEGs associated with innate immune response and lymphocyte homing.

	Pathway	id	Gene Symbol	Module
Antiviral innate immune response	Phagosome	ncbi_101804485	*MHC-2*	mediumpurple3
	Cytosolic DNA-sensing pathway	ncbi_101789567	*RIG-1*	coral2
		ncbi_101800076	*MDA5*	coral2
		ncbi_101792382	*LGP2*	coral2
		ncbi_101797757	*cGAS*	coral2
		ncbi_101799156	*STING*	coral2
		ncbi_101795904	*IRF7*	coral2
	Cytokine-cytokine receptor interaction	ncbi_101798321	*IL-6*	coral2
		ncbi_101798847	*IFN-α*	coral2
		ncbi_101796052	*IFN-β*	coral2
	Jak-STAT signaling pathway	ncbi_101802227	*STAT1*	coral2
	Cytokine-cytokine receptor interaction	ncbi_101801826	*IL-10*	coral2
		ncbi_101790246	*IL-22*	coral2
Lymphocyte migration and homing	Cell adhesion molecules (CAMs) /Intestinal immune network for IgA production	ncbi_101791924	*VCAM1*	coral2
		XLOC_020773	*MAdCAM1*	coral2
	Cell adhesion molecules (CAMs)	ncbi_101804859	*ICAM1*	coral2
		ncbi_101799485	*ITGA4*	mediumpurple3
		ncbi_101796803	*ITGB2*	coral2
	Cytokine-cytokine receptor interaction	ncbi_101790039	*CCL19*	coral2
		ncbi_101793244	*CCL21*	coral2
		ncbi_101789878	*CCR7*	mediumpurple3
		ncbi_101800424	*CCL5*	coral2
		ncbi_101800429	*CCR5*	coral2
		ncbi_101800964	*IL-8(CXCL13)*	coral2
		ncbi_101798696	*CXCR5*	mediumpurple3
	Intestinal immune network for IgA production	ncbi_101792342	*CXCL12*	mediumpurple3
		ncbi_101802610	*CCR9*	mediumpurple3

virus invasion, while MHC-2 was contributed to antigen presentation. The other 6 DEGs belonging to cytokine-cytokine receptor interaction (i.e. pro-inflammatory cytokine IL-6 and anti-inflammatory cytokine IL-10, IL-22, IFN-α, IFN-β and STAT1 from Jak-STAT signaling pathway) were related to inflammation. The remaining 10 DEGs (adhesion molecules VCAM1, MAdCAM1, ICAM1 and their ligands integrin α4, integrin β2 and chemokines CCL19/CCL21/CCR7, IL-8(CXCL13)/CXCR5) were associated with lymphocyte migration and homing. Moreover, DEGs that related to virus invasion, cytokines and lymphocytes migration were mostly found in coral2 module.

3.3.6. Validation of RNA-seq results by RT-qPCR

To validate the identified DEGs from RNA-Seq, 23 DEGs and DTMUV gene were selected and subjected to RT-qPCR analysis. Furthermore, the validated RT-qPCR results were compared with the read counts calculated by FPKM method. The mRNA expression patterns of these genes were found to be consistent with the relative changes in transcript abundance obtained from RNA-Seq (Fig. 10), suggesting the highly accuracy and quality of RNA-seq analysis. The expression level of virus gene increased slowly between 2 hpi and 12 hpi, and significantly at 1 dpi and 3 dpi, followed a rapid decline. Such expression pattern was similar to that of genes in coral2 module (Fig. 11).

3.3.7. Confirmation of RNA-seq findings by Western blotting

The expression levels of the 14 proteins were detected by Western blotting using β-actin as an inner control. The results indicated that the proteins expression patterns of these genes were similar to the relative changes in transcript abundance obtained from RNA-Seq (Fig. 10). Compared to those genes, the expression levels of certain proteins were slightly delayed.

4. Discussion

The Flavivirus genus of the Flaviviridae family contains more than 70 viruses, including dengue virus, Japanese encephalitis virus, West Nile virus, etc. (King et al., 2007). Flavivirus generally spreads via the bloodstream, and leads to viremia after infecting humans and animals. Most flaviviruses firstly appear to accumulate within the spleen (Carson et al., 2006; Garcia et al., 2011; Kato et al., 2014), and eventually causes systemic viral injury and chronic disease. DTMUV, a novel member of flavivirus genus, exhibits the common features of pathogenicity (Wu et al., 2014). The spleen contains the highest viral loads compared to other organs (Jiang et al., 2012; Wu et al., 2014). In our previous work (unpublished) on the dynamical distribution of DTMUV in duck spleen, 10^4 $TCID_{50}$ dose of DTMUV strain XZ-2012 has been detected at 2 hpi, reached the replication peak at 3dpi, and then gradually decreased until complete elimination at 18dpi. Therefore, in this study, seven infected time points from 2 hpi to 18 dpi were selected to decipher the pathogenic mechanisms of DTMUV in the spleen.

KEGG enrichment analysis revealed that DEGs were mainly enriched in pathways related to viral invasion, immune response and lymphocytes migration, including “Cytosolic DNA-sensing pathway”, “RIG-I-like receptor signaling pathway”, “Cytokine-cytokine receptor interaction”, “Phagosome”, et al. The results indicated that DTMUV invaded host cells at the early period after infection, activated immune response in the spleen by recruiting lymphocytes and recovered.

In previous study on duck embryo fibroblasts (DEFs) infected with DTMUV (Yu et al., 2018), DEGs were considerably enriched in immune-relevant pathways, DTMUV infection induces strong proinflammatory/antiviral effects with enormous production of cytokines. However, these cytokines could not protect DEFs against viral attack. Host innate immune response plays an important role in the early stage of pathogen infection. Pattern recognition receptors (PRRs) such as RIG-I like receptors (RLRs), including retinoic acid induced gene-I (RIG-I), melanoma differentiation associated gene 5 (MDA5) and laboratory of genetics and physiology-2 (LGP2), are the key components of the host innate immune system, which can recognize the conservative elements of pathogenic RNA viruses (Janeway and Medzhitov, 2002). Downstream signal cascade reactions are initiated through mitochondrial antiviral signaling protein (MAVS) and Interferon regulatory factor 3/7 (IRF3/7) to synthesize type I interferon and pro-inflammatory cytokines (Takeuchi and Akira, 2010). Flavivirus can induce innate immune response by producing type-I interferon IFN-α/β and pro-inflammatory factor IL-6, and activating RIG-I/MDA5-MAVS-IRF7/NF-κB and Jak-STAT signaling pathways (Fredericksen et al., 2008; Green et al., 2014;

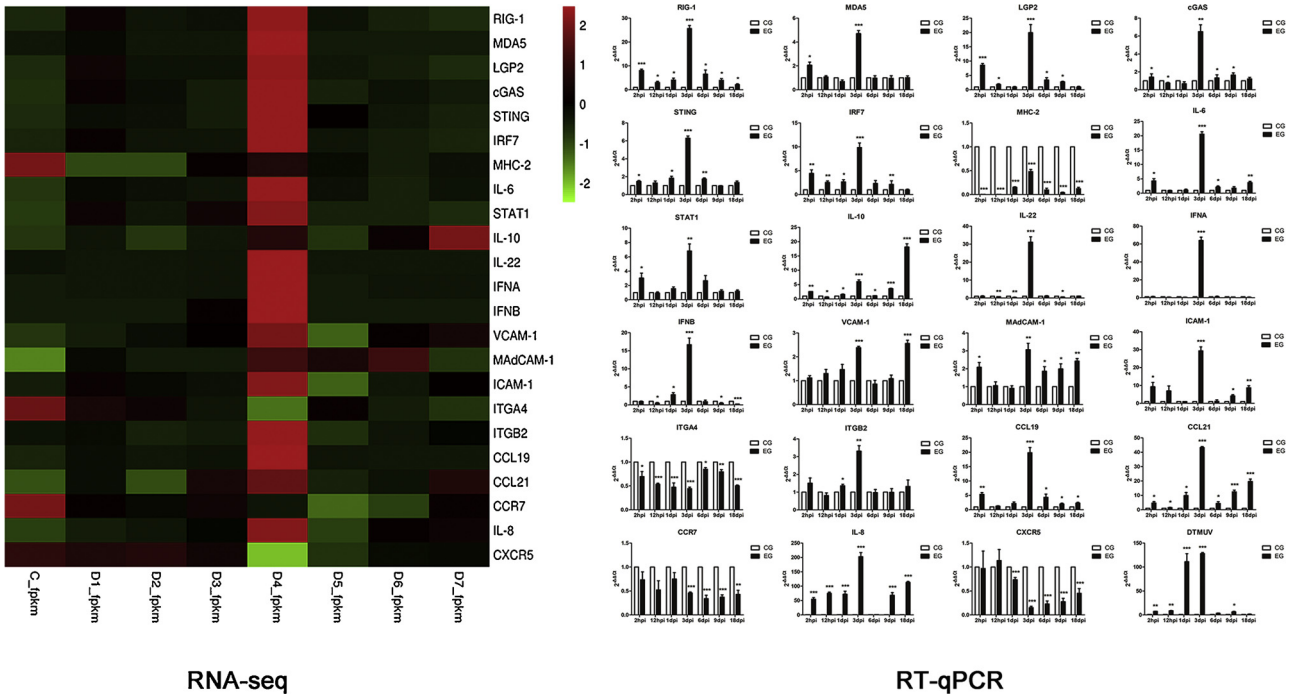

Fig. 10. RT-qPCR results (a) and the heat map comparison of DEGs between RNA-seq and RT-qPCR (b). (a) The x-coordinate represents the eight samples; the y-coordinate represents the relative expression of genes. (b) The red color represents high expression; the green color represents low expression. (For interpretation of the references to colour in this figure legend, the reader is referred to the web version of this article).

Li, 2017). Through RNA-seq, we found that the expression levels of PRRs RIG-I, MDA5, LGP2 and IRF7 were slightly upregulated during DTMUV invasion in the spleen, while IFN-α/β was not involved in this stage. These results were further verified by RT-qPCR and Western blotting. Flavivirus invades into host cells by binding with PRRs and endocytosis to form endosomes (Chu and Ng, 2004). Subsequently, viral ssRNA is released into the cells for replication and assembly (Mukhopadhyay et al., 2005; Rodenhuis-Zybert et al., 2010). Under TEM, late endosomes were observed during the early infection period, while MHC-2 expression was significantly downregulated as shown by RNA-seq. These findings suggest that DTMUV may activate phagosome pathway by endocytosis and inhibit the expression of MHC-2 during immune evasion. IL-6, a major pro-inflammatory cytokine, was significantly upregulated from 12 hpi to 3 dpi of DTMUV. At the same time, the morphological and cellular lesions of infected spleen were observed. The overexpression of proinflammatory cytokine IL-6 may damage the host (Li et al., 2015). Therefore, it was suggested that IL-6 caused status marmoratus. At 3 dpi, the expression levels of PRRs RIG-1, MDA5, LGP2 and IRF7 were significantly upregulated, and subsequently induced downstream IFN-α/β and STAT-1 of Jak-STAT signaling pathway. IL-10, an anti-inflammatory cytokine, was significantly upregulated during later stage infection. Therefore, IFN-α/β and IL-10 are essential for the clearance of infectious virus from the spleen. In addition, cGAS and STING in cGAS-STING signaling pathway of sensing

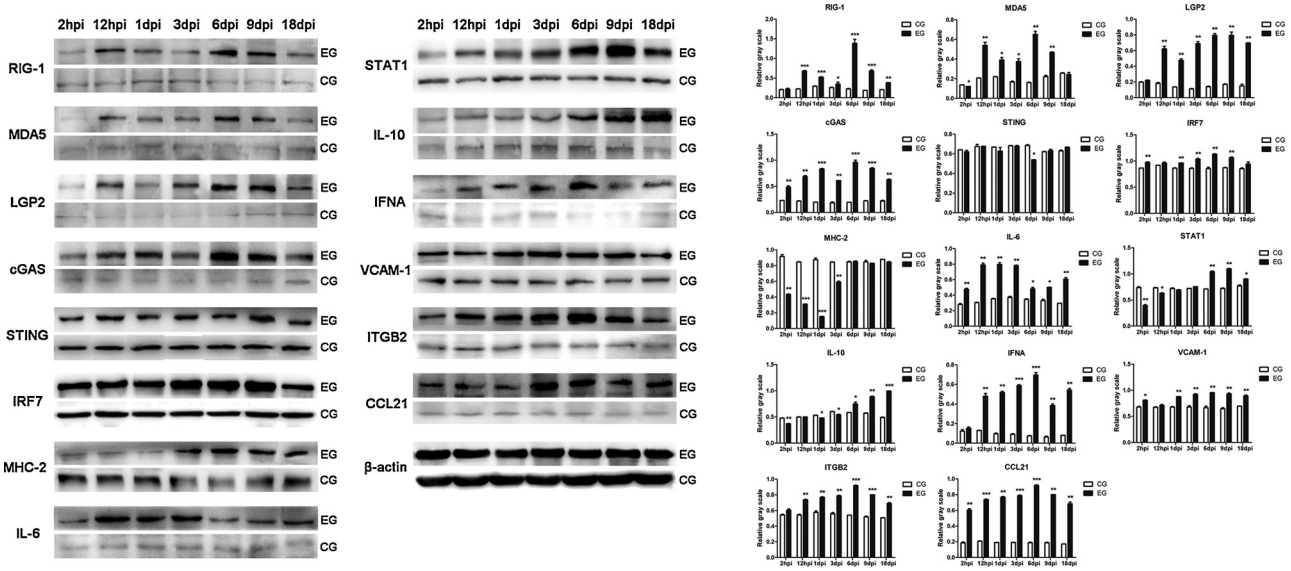

Fig. 11. Western blotting results. The bar chart value represents the grayscale value of the protein strip. The x-coordinate represents the eight samples; the y-coordinate represents the relative grayscale value.

DNA virus (Ma and Damania, 2016) exhibited a co-expression relationship with RLRs. Therefore, we speculated that DTMUV can be reversely transcribed.

Lymphocytes often migrate to the peripheral lymphoid organs via the specialized high endothelial venule (HEV) (Girard and Springer, 1995). In mammals, lymphocytes enter the white pulp of spleen through the marginal zone due to lack of HEVs (Lu and Cyster, 2002). However, the structural organization of avian spleen is devoid of the marginal zone. A previous morphological study has reported that the sheathed capillary in chicken spleen is a HEV-like vessel (Zhang et al., 2017). Several regulators factors of lymphocyte homing such as CAMs (e.g. ICAM-1, VCAM-1 and MAdCAM-1), the receptors expressed on lymphocytes (e.g. integrin αLβ2, integrin α4β1 and integrin α4β7), as well as specific chemokines and receptors (e.g. CXCL12/CXCR4, CCL25/CCR9 and CCL28/CCR10) may play critical roles in transendothelial migration in mammals and chickens (Abdala-Valencia et al., 2011; de Chateau et al., 2001; Imai et al., 2010; Muller, 2011, 2014; Rothlein et al., 2011). Our previous study has found that the cuboidal-shaped endothelial cells of the sheathed capillaries in duck spleen are high endothelial cells (HECs) and the pathways for lymphocyte migrating into spleen (Sun et al., 2018). Noticeably, VCAM-1, MAdCAM-1 and ICAM-1 were significantly upregulated at 3 dpi, as well as the increased number of lymphocytes. These results suggest that a large number of lymphocytes migrated into the spleen across the sheathed capillary. However, RNA-seq results showed that the expression levels of *integrin α4*, *integrin β1*, *CXCL12/CXCR4*, *CCR9* and *CCR10* exhibited no significant co-expression relationship with CAMs. Meanwhile, the expression of *integrin β7*, *integrin αL*, *CCL25* and *CCL28* were not detected in the mallard (*Anas platyrhynchos*) genome, suggesting the different mechanisms of lymphocyte homing among duck, chicken and mammals. On the contrary, *CCL19*, *CCL21* and *integrin β2* were co-expressed with CAMs in infected duck spleen, suggesting that these genes may govern lymphocyte homing to the spleen (Hauser and Legler, 2016).

Furthermore, in this study, the neuroactive ligand-receptor interaction pathway related to the nervous system was significantly enriched starting from 1 dpi. Clarke et al. found that this pathway is enriched during Japanese encephalitis virus infection in mice (Clarke et al., 2014), which is consistent with the current results. Therefore, we speculated that DTMUV may exert the same pathogenetic infection mechanism as JEV and can affect the nervous system.

5. Conclusions

In summary, the invasion process of DTMUV in duck spleen was divided into several phases based on the underlying cellular and molecular mechanisms. At the initial stage, DTMUV might invade into the spleen via inhibiting MHC-2 expression and induce lesions via activating IL-6 expression. Additionally, the expression levels of PRRs and downstream antiviral cytokines type I IFN in RIG-I/MDA5-MAVS-IRF7 pathway were upregulated in the duck spleen. Eventually, a large number of lymphocytes migrated into spleen and played an important role in resisting DTMUV infection. These novel findings contribute to a better understanding of avian immune response to viral infection, and the underling mechanisms deserve more attention in future.

Ethics approval and consent to participate

The sampling procedures were approved by the College of Veterinary Medicine, Nanjing Agricultural University. The study protocol was approved by the Science and Technology Agency of Jiangsu Province (SYXK (SU) 2010-0005).

Competing interests

The authors declare that there are no conflicts of interest.

Funding

This study was supported by the National Natural Science Foundation of China (No. 31672505 and 31872433) and Priority Academic Program for Development of Jiangsu Higher Education Institution, China.

Authors' contributions

The authors have made the following declarations about their contributions: Xuejing Sun and Qiusheng Chen designed the experiments. Xuejing Sun performed most of the experimental work with the assistance of Wenqian Li, Enxue Liu, Xindong Wang, Taozhi Wang. Xuejing Sun analyzed data of RNA-seq and wrote the manuscript with the assistance of Haixiang Huang. Yonghong Shi provided the equipment of TEM. Qiusheng Chen and Ping Yang revised the paper. All authors read and approved the final manuscript.

Acknowledgements

We thank Prof. Ruibing Cao from Nanjing Agricultural University for providing the isolated and purified DTMUV strain XZ-2012.

Appendix A. Supplementary data

Supplementary material related to this article can be found, in the online version, at doi:https://doi.org/10.1016/j.vetmic.2018.12.003.

References

Abdala-Valencia, H., Berdnikovs, S., Cook-Mills, J.M., 2011. Mechanisms for vascular cell adhesion molecule-1 activation of ERK1/2 during leukocyte trans endothelial migration. PLoS One 6.

Cao, Z.Z., Zhang, C., Liu, Y.H., Ye, W.C., Han, J.W., Ma, G.M., Zhang, D.D., Xu, F., Gao, X.H., Tang, Y., Shi, S.H., Wan, C.H., Zhang, C., He, B., Yang, M.J., Lu, X.H., Huang, Y., Diao, Y.X., Ma, X.J., Zhang, D.B., 2011. Tembusu virus in ducks, China. Emerg. Infect. Dis. 17, 1873–1875.

Carson, P.J., Konewko, P., Wold, K.S., Mariani, P., Goli, S., Bergloff, P., Crosby, R.D., 2006. Long-term clinical and neuropsychological outcomes of West Nile virus infection. Clin. Infect. Dis. 43, 723–730.

Chen, S.L., Chen, S.Y., Wang, S., Lin, F.Q., Jiang, B., Cheng, X.X., Huang, M.Q., Zhu, X.L., Li, Z.L., 2011. Isolation and identification of new flaviviruses causing reduction on egg-laying in chicken. Fujian J. Agric. Sci. 26, 170–174.

Chu, Y.J., Corey, D.R., 2012. RNA sequencing: platform selection, experimental design, and data interpretation. Nucleic Acid Ther. 22, 271–274.

Chu, J.J.H., Ng, M.L., 2004. Infectious entry of West Nile virus occurs through a clathrin-mediated endocytic pathway. J. Virol. 78, 10543–10555.

Clarke, P., Leser, J.S., Bowen, R.A., Tyler, K.L., 2014. Virus-induced transcriptional changes in the brain include the differential expression of genes associated with interferon, apoptosis, interleukin 17 receptor a, and glutamate signaling as well as flavivirus-specific upregulation of tRNA synthetases. Mbio 5.

de Chateau, M., Chen, S.Q., Salas, A., Springer, T.A., 2001. Kinetic and mechanical basis of rolling through an integrin and novel Ca2+-dependent rolling and Mg2+-dependent firm adhesion modalities for the alpha 4 beta 7-MAdCAM-1 interaction. Biochemistry 40, 13972–13979.

Fredericksen, B.L., Keller, B.C., Fornek, J., Katze, M.G., Gale, M., 2008. Establishment and maintenance of the innate antiviral response to west nile virus involves both RIG-I and MDA5 signaling through IPS-1. J. Virol. 82, 609–616.

Garcia, G., Gonzalez, N., Perez, A.B., Sierra, B., Aguirre, E., Rizo, D., Izquierdo, A., Sanchez, L., Diaz, D., Lezcay, M., Pacheco, B., Hirayama, K., Guzman, M.G., 2011. Long-term persistence of clinical symptoms in dengue-infected persons and its association with immunological disorders. Int. J. Infect. Dis. 15, E38–E43.

Girard, J.P., Springer, T.A., 1995. High endothelial venules (Hevs) - specialized endothelium for lymphocyte migration. Immunol. Today 16, 449–457.

Green, A.M., Beatty, P.R., Hadjilaou, A., Harris, E., 2014. Innate immunity to dengue virus infection and subversion of antiviral responses. J. Mol. Biol. 426, 1148–1160.

Hauser, M.A., Legler, D.F., 2016. Common and biased signaling pathways of the chemokine receptor CCR7 elicited by its ligands CCL19 and CCL21 in leukocytes. J. Leukoc. Biol. Suppl. 99, 869–882.

Hollender, C.A., Kang, C.Y., Darwish, O., Geretz, A., Matthews, B.F., Slovin, J., Alkharouf, N., Liu, Z.C., 2014. Floral transcriptomes in Woodland Strawberry uncover developing receptacle and anther gene networks. Plant Physiol. 165, 1062–1075.

Huang, X.M., Han, K.K., Zhao, D.M., Liu, Y.Z., Zhang, J.F., Niu, H.M., Zhang, K.N., Zhu, J.N., Wu, D.M., Gao, L., Li, Y., 2013. Identification and molecular characterization of a novel flavivirus isolated from geese in China. Res. Vet. Sci. 94, 774–780.

Imai, Y., Shimaoka, M., Kurokawa, M., 2010. Essential roles of VLA-4 in the

hematopoietic system. Int. J. Hematol. 91, 569–575.
Janeway, C.A., Medzhitov, R., 2002. Innate immune recognition. Annu. Rev. Immunol. 20, 197–216.
Jiang, T., Liu, J., Deng, Y.Q., Su, J.L., Xu, L.J., Liu, Z.H., Li, X.F., Yu, X.D., Zhu, S.Y., Gao, G.F., Qin, E.D., Qin, C.F., 2012. Development of RT-LAMP and real-time RT-PCR assays for the rapid detection of the new duck Tembusu-like BYD virus. Arch. Virol. 157, 2273–2280.
Kato, N., Sejima, H., Ueda, Y., Mori, K., Satoh, S., Dansako, H., Ikeda, M., 2014. Genetic characterization of hepatitis C virus in long-term RNA replication using Li23 cell culture systems. PLoS One 9.
Kim, D., Pertea, G., Trapnell, C., Pimentel, H., Kelley, R., Salzberg, S.L., 2013. TopHat2: accurate alignment of transcriptomes in the presence of insertions, deletions and gene fusions. Genome Biol. 14.
King, N.J.C., Getts, D.R., Getts, M.T., Rana, S., Shrestha, B., Kesson, A.M., 2007. Immunopathology of flavivirus infections. Immunol. Cell Biol. 85, 33–42.
Langfelder, P., Horvath, S., 2008. WGCNA: an R package for weighted correlation network analysis. BMC Bioinformatics 9.
Li, N., 2017. Host Innate Immune Response Induced by Duck Tembusu Virus and the Interaction Between the Virus and RLR-mediated Signaling Pathway. Shandong Agricultural University.
Li, N., Wang, Y., Li, R., Liu, J.Y., Zhang, J.Z., Cai, Y.M., Liu, S.D., Chai, T.J., Wei, L.M., 2015. Immune responses of ducks infected with duck Tembusu virus. Front. Microbiol. 6.
Lu, T.T., Cyster, J.G., 2002. Integrin-mediated long-term B cell retention in the splenic marginal zone. Science 297, 409–412.
Ma, Z., Damania, B., 2016. The cGAS-STING defense pathway and its counteraction by viruses. Cell Host Microbe 19, 150–158.
Maher, C.A., Kumar-Sinha, C., Cao, X.H., Kalyana-Sundaram, S., Han, B., Jing, X.J., Sam, L., Barrette, T., Palanisamy, N., Chinnaiyan, A.M., 2009. Transcriptome sequencing to detect gene fusions in cancer. Nature 458, 97–U99.
Mukhopadhyay, S., Kuhn, R.J., Rossmann, M.G., 2005. A structural perspective of the Flavivirus life cycle. Nat. Rev. Microbiol. 3, 13–22.
Muller, W.A., 2011. Mechanisms of leukocyte transendothelial migration. Annu. Rev. Pathol. Mech. Dis. 6 (6), 323–344.
Muller, W.A., 2014. How endothelial cells regulate transendothelial migration of leukocytes: molecules and mechanisms. Therm. Sens. 74, 335–355.
Reed, L.J., Muench, H., 1938. A simple method of estimation of fifty percent endpoint. Am. J. Epidemiol. 27, 493–497.
Rodenhuis-Zybert, I.A., Wilschut, J., Smit, J.M., 2010. Dengue virus life cycle: viral and host factors modulating infectivity. Cell. Mol. Life Sci. 67, 2773–2786.
Rothlein, R., Dustin, M.L., Marlin, S.D., Springer, T.A., 2011. A human intercellular adhesion molecule (Icam-1) distinct from Lfa-1. J. Immunol. 186, 5034–5038.
Samuel, M.A., Diamond, M.S., 2006. Pathogenesis of West Nile Virus infection: a balance between virulence, innate and adaptive immunity, and viral evasion. J. Virol. 80, 9349–9360.
Sejvar, J.J., Haddad, M.B., Tierney, B.C., Campbell, G.L., Marfin, A.A., Van Gerpen, J.A., Fleischauer, A., Leis, A.A., Stokic, D.S., Petersen, L.R., 2003. Neurologic manifestations and outcome of West Nile virus infection. Jama 290, 511–515.
Su, J.L., Li, S.A., Hu, X.D., Yu, X.L., Wang, Y.Y., Liu, P.P., Lu, X.S., Zhang, G.Z., Hu, X.Y., Liu, D., Li, X.X., Su, W.L., Lu, H., Mok, N.S., Wang, P.Y., Wang, M., Tian, K.G., Gao, G.F., 2011. Duck egg-drop syndrome caused by BYD virus, a new tembusu-related flavivirus. PLoS One 6.
Sun, X., Liu, E., Wang, T., Zhang, Q., Yang, P., Ahmed, N., Zhao, Q., Chen, Q., 2018. The novel histological evidence of the blood-spleen barrier in duck (Anas platyrhynchos). Histol. Histopathol. 18019.
Takeuchi, O., Akira, S., 2010. Pattern recognition receptors and inflammation. Cell 140, 805–820.
Teng, Q., Yan, P., Zhang, X., Yan, L., Li, Z., 2010. A novel flavivirus causing duck egg drops and death. Chin. J. Anim. Infect. Dis.
Ti, J.F., Zhang, L., Li, Z.J., Zhao, D.D., Zhang, Y., Li, F., Diao, Y.X., 2015. Effect of age and inoculation route on the infection of duck Tembusu virus in Goslings. Vet. Microbiol. 181, 190–197.
Trapnell, C., Williams, B.A., Pertea, G., Mortazavi, A., Kwan, G., van Baren, M.J., Salzberg, S.L., Wold, B.J., Pachter, L., 2010. Transcript assembly and quantification by RNA-Seq reveals unannotated transcripts and isoform switching during cell differentiation. Nat. Biotechnol. 28, 511–U174.
Wan, C.H., Shi, S.H., Cheng, L.F., Chen, H.M., Fu, G.H., Zhang, D.B., Lin, F., Lin, J.S., Huang, Y., 2010. A newly identified Flavivirus Virus causing abrupt egg-laying reduction in ducks. Fujian J. Agric. Sci. 25, 663–666.
Wan, C.H., Huang, Y., Fu, G.H., Shi, S.H., Cheng, L.F., Chen, H.M., 2012. Complete genome sequence of avian tembusu-related virus strain WR isolated from white Kaiya ducks in Fujian, China. J. Virol. 86 10912-10912.
Wang, Z., Gerstein, M., Snyder, M., 2009. RNA-Seq: a revolutionary tool for transcriptomics. Nat. Rev. Genet. 10, 57–63.
Wang, Y., Wang, J.M., Cao, R.B., 2015. Isolation and gene variation character of duck Tembusu virus strain XZ-2012. J. Nanjing Agric. Univ. 38, 446–452.
Wu, L., Liu, J., Chen, P., Jiang, Y., Ding, L., Lin, Y., Li, Q., He, X., Chen, Q., Chen, H., 2014. The sequential tissue distribution of duck Tembusu virus in adult ducks. Biomed Res. Int. 2014, 703930.
Yan, P.X., Zhao, Y.S., Zhang, X., Xu, D.W., Dai, X.G., Teng, Q.Y., Yan, L.P., Zhou, J.W., Ji, X.W., Zhang, S.M., Liu, G.Q., Zhou, Y.J., Kawaoka, Y., Tong, G.Z., Li, Z.J., 2011. An infectious disease of ducks caused by a newly emerged Tembusu virus strain in mainland China. Virology 417, 1–8.
Yu, G.L., Lin, Y., Tang, Y., Diao, Y.X., 2018. Comparative transcriptomic analysis of immune-related gene expression in duck embryo fibroblasts following duck tembusu virus infection. Int. J. Mol. Sci. 19.
Yun, T., Ye, W.C., Ni, Z., Zhang, D.B., Zhang, C., 2012a. Identification and molecular characterization of a novel flavivirus isolated from Pekin ducklings in China. Vet. Microbiol. 157, 311–319.
Yun, T., Zhang, D.B., Ma, X.J., Cao, Z.Z., Chen, L., Ni, Z., Ye, W.C., Yu, B., Hua, J.G., Zhang, Y., Zhang, C., 2012b. Complete genome sequence of a novel flavivirus, duck tembusu virus, isolated from ducks and geese in China. J. Virol. 86, 3406–3407.
Zhang, D.J., Shen, X.H., Zhao, R.H., D, Y., Hu, X.M., Pan, X.C., Hou, H.Y., Zhou, X.L., Zhu, C.M., 2015. Pathogenicity study of duck tembusu virus in laying hens. China. Poultry 37, 13–17.
Zhang, Q., Waqas, Y., Yang, P., Sun, X.J., Liu, Y., Ahmed, N., Chen, B., Li, Q.F., Hu, L.S., Huang, Y.F., Chen, H., Hu, B., Chen, Q.S., 2017. Cytological study on the regulation of lymphocyte homing in the chicken spleen during LPS stimulation. Oncotarget 8, 7405–7419.